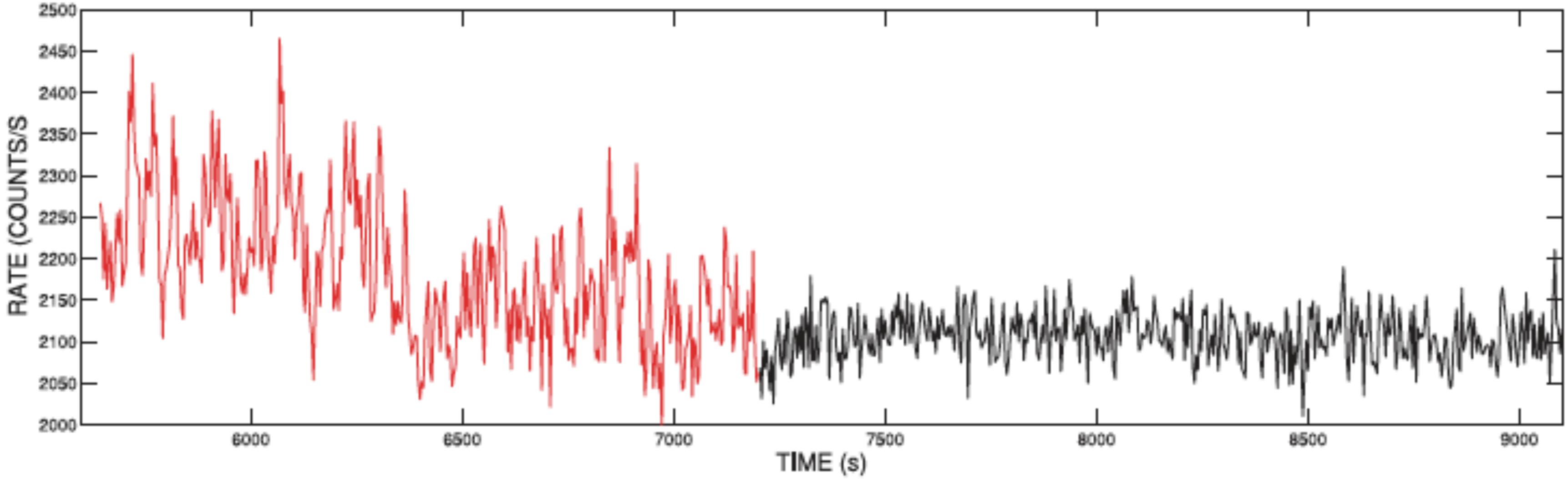

Fast variability of X-ray binaries

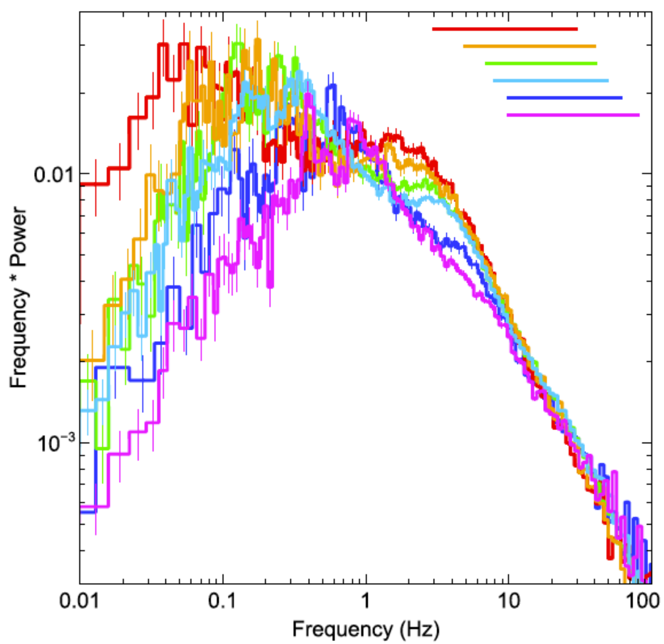

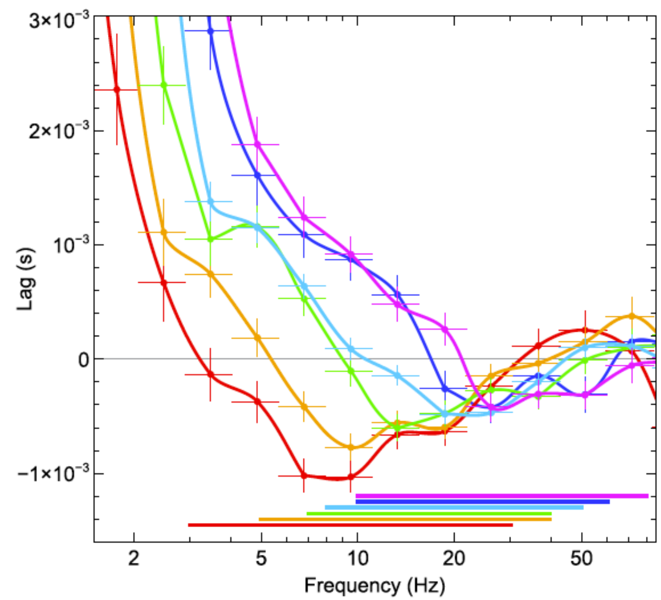

Shot noise vs propagating fluctuations

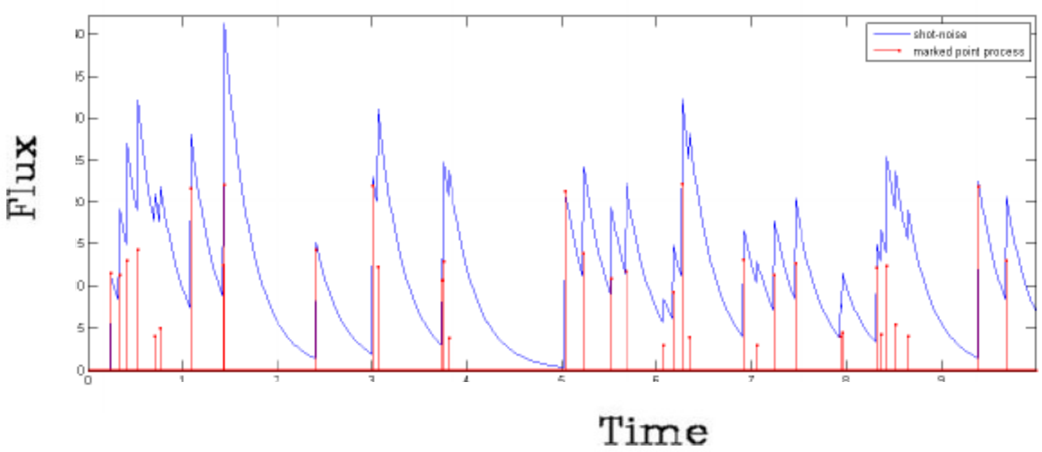

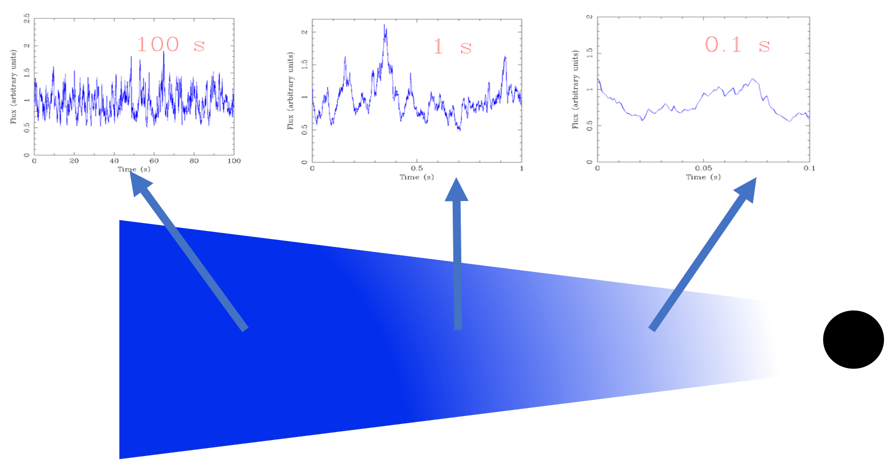

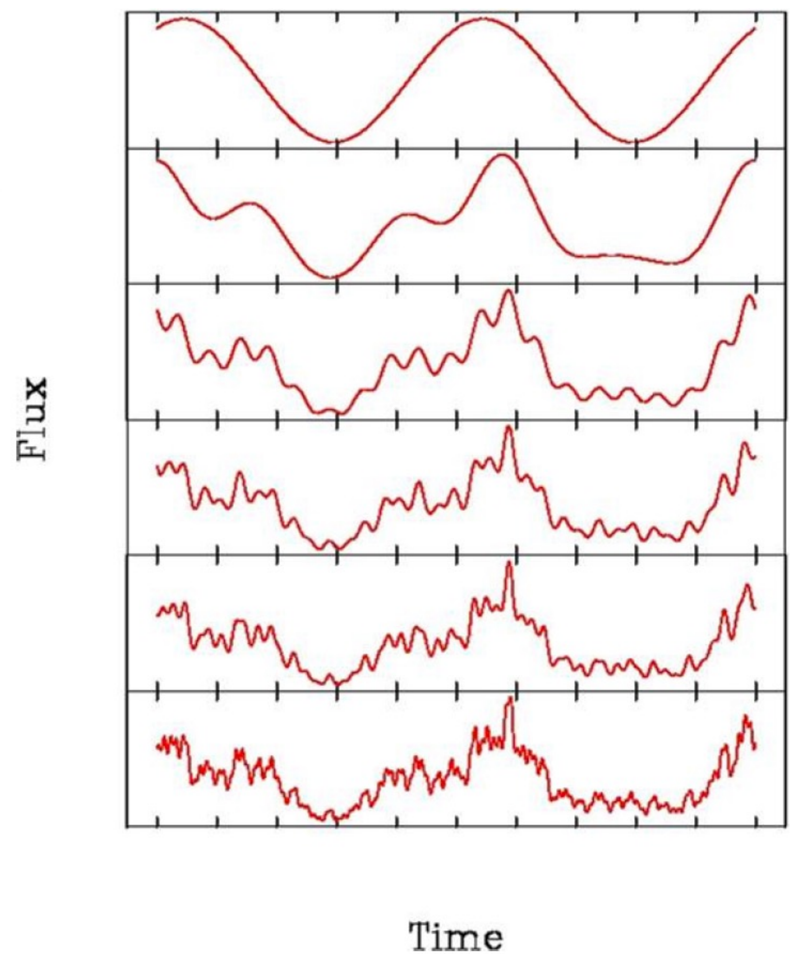

Truncated disc and propagation model

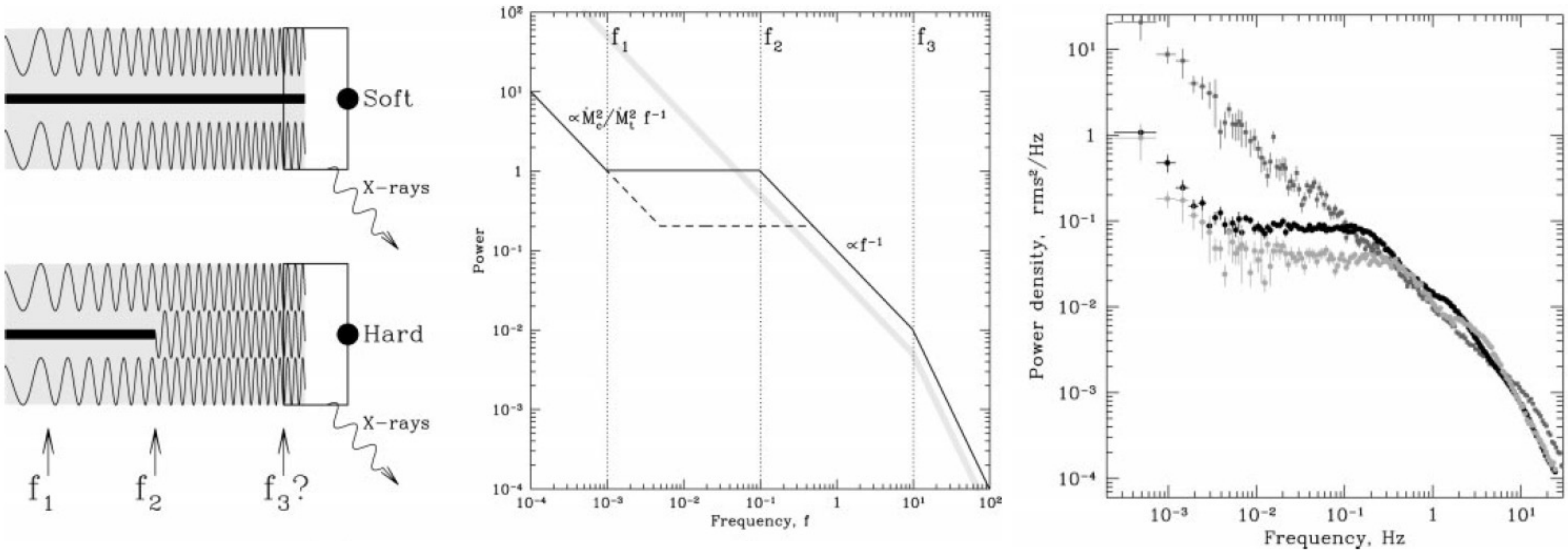

PSD shape changes as the source makes transition towards the soft spectral state. The idea of a stable disc and fluctuating corona. Data from high-mass X-ray binary Cyg X-1.

Truncated disc and propagation model

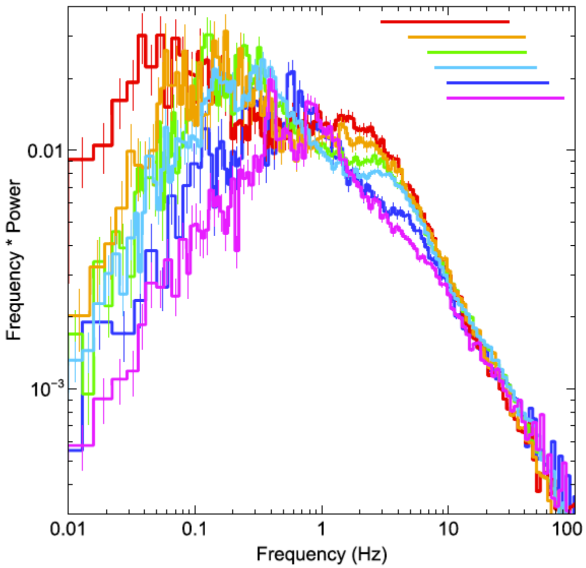

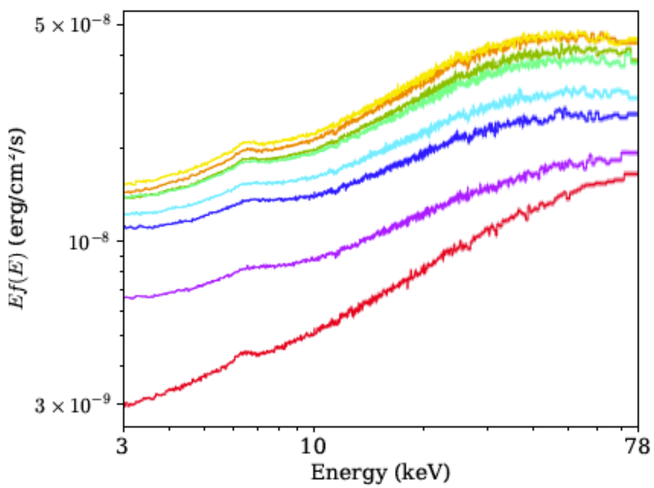

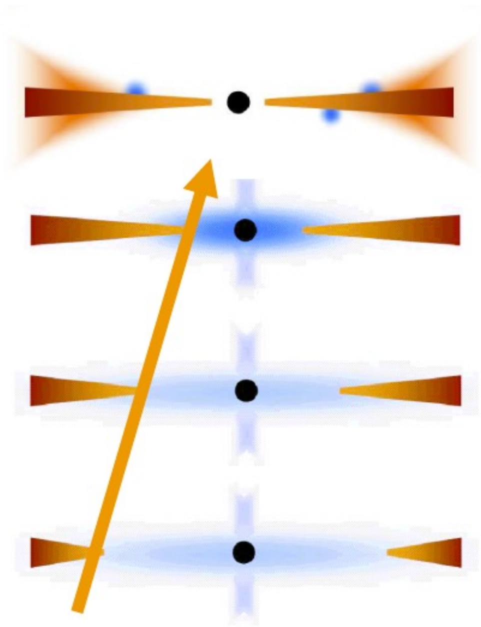

PSD has a low-frequency break which moves to higher *f* as the sources softens. Consistent with the picture where fluctuations arising from outer parts of the hot accretion flow becomes damped as the flow shrinks. Data from low-mass X-ray binary MAXI J1820+070.

Cross-spectrum

- Consider two light curves, in “soft” and “hard” energy bands, *s(t)* and *h(t)*. Let S_j and H_j be their discrete Fourier transforms

$$S_j = |S_j| e^{i\varphi_{j,s}}, H_j = |H_j| e^{i\varphi_{j,h}}$$

- (!) Recall that for real signal we have $S_j = S^*_{-j}$
- Phases themselves $\varphi_{j,h}, \varphi_{j,s}$ are usually not interesting, but their difference $\Delta\varphi_j = \varphi_{j,h} - \varphi_{j,s}$ is.
- The cross-spectrum is defined as

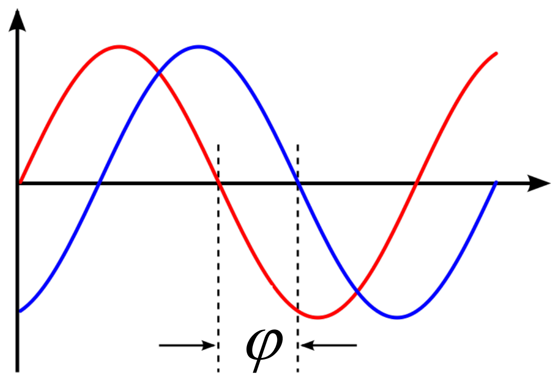

$$C_j = S_j^* H_j = |S_j||H_j| e^{i(\varphi_{j,h} - \varphi_{j,s})} = |S_j||H_j| e^{i\Delta\varphi_j}$$

- We define the Fourier time lag as $\Delta t(f) = \Delta\varphi(f)/2\pi f$
- One should note that both phase and time lags are generally functions of the Fourier frequency.

Time lags in Cyg X-1. Shot noise model

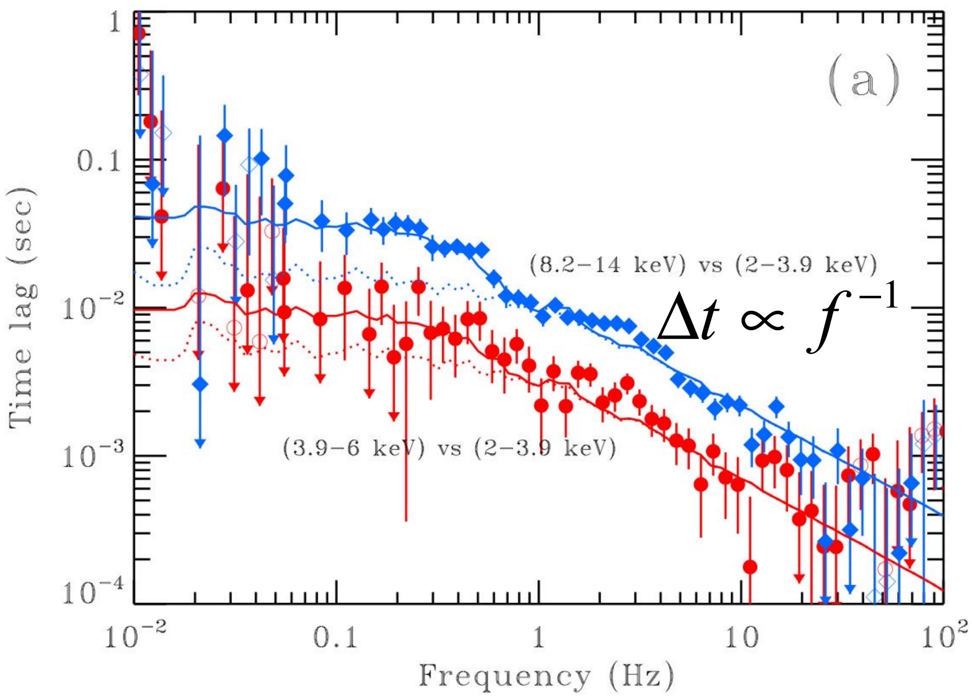

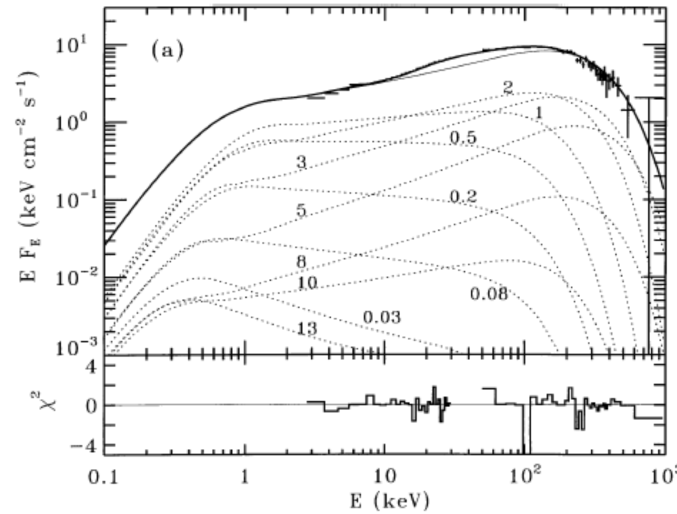

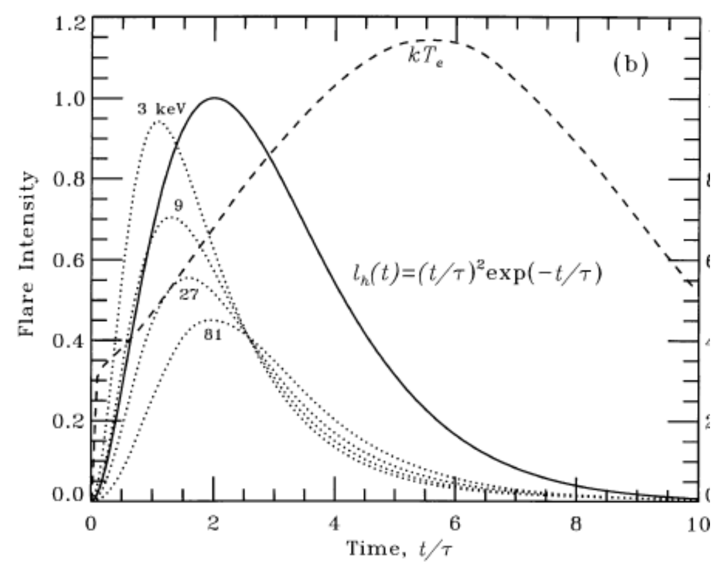

Time lags are function of frequency, can be explained by spectral variability.

$$g(t) = \begin{cases} e^{-t/\tau}, & t \geq 0 \\ 0, & t < 0 \end{cases} \qquad p(\tau) = \begin{cases} \tau^{-\eta}, & \tau_{\min} < \tau < \tau_{\max} \\ 0, & \text{otherwise} \end{cases}$$

Time lags in Cyg X-1. Shot noise model

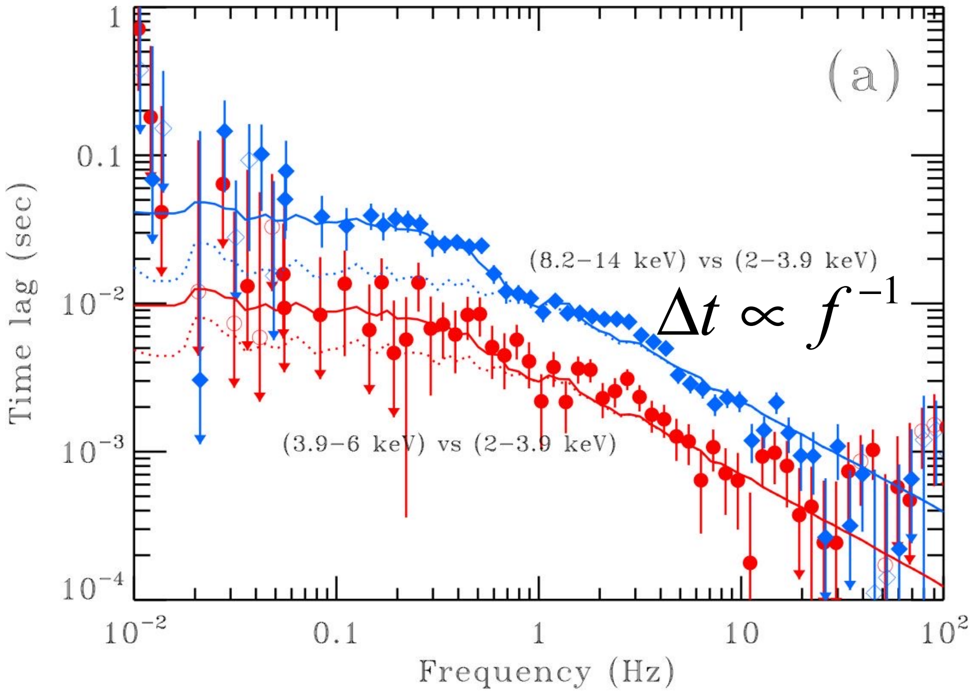

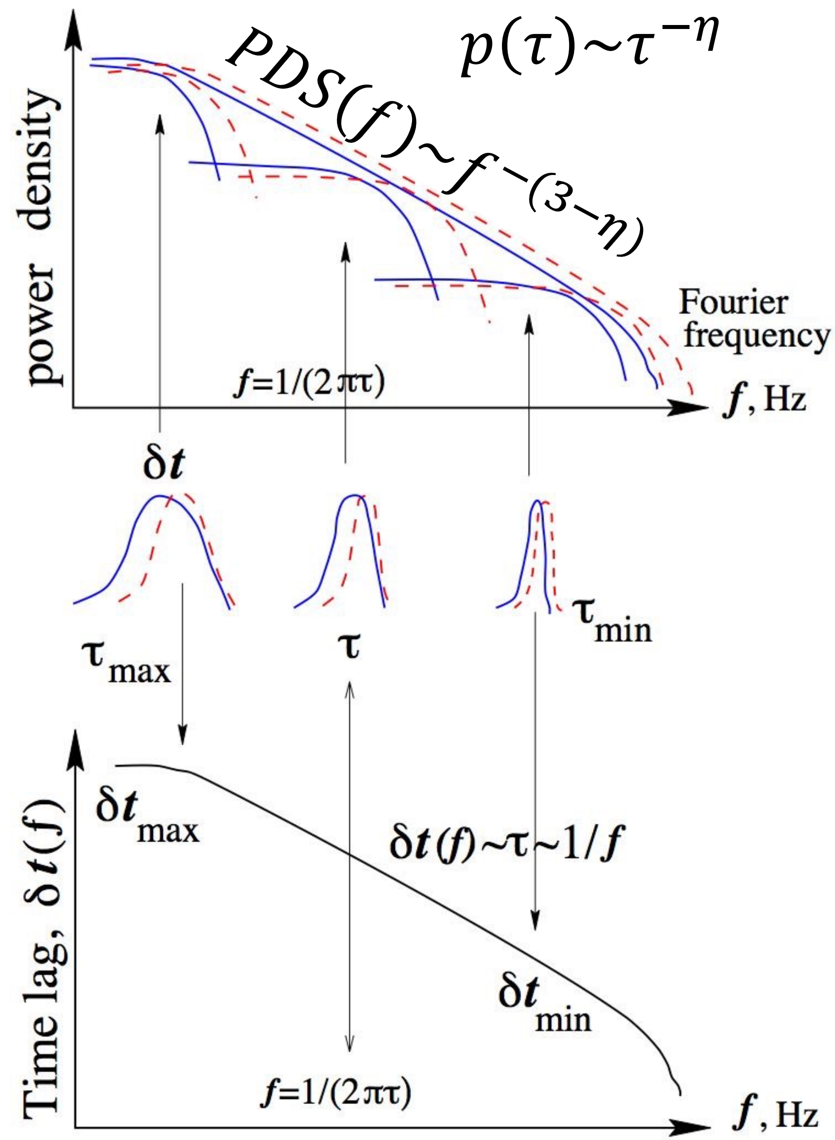

Time lags are function of frequency, can be explained by spectral variability.

$$g(t) = \begin{cases} e^{-t/\tau}, & t \geq 0 \\ 0, & t < 0 \end{cases} \qquad p(\tau) = \begin{cases} \tau^{-\eta}, & \tau_{\min} < \tau < \tau_{\max} \\ 0, & \text{otherwise} \end{cases}$$

Time lags in Cyg X-1. Propagation model

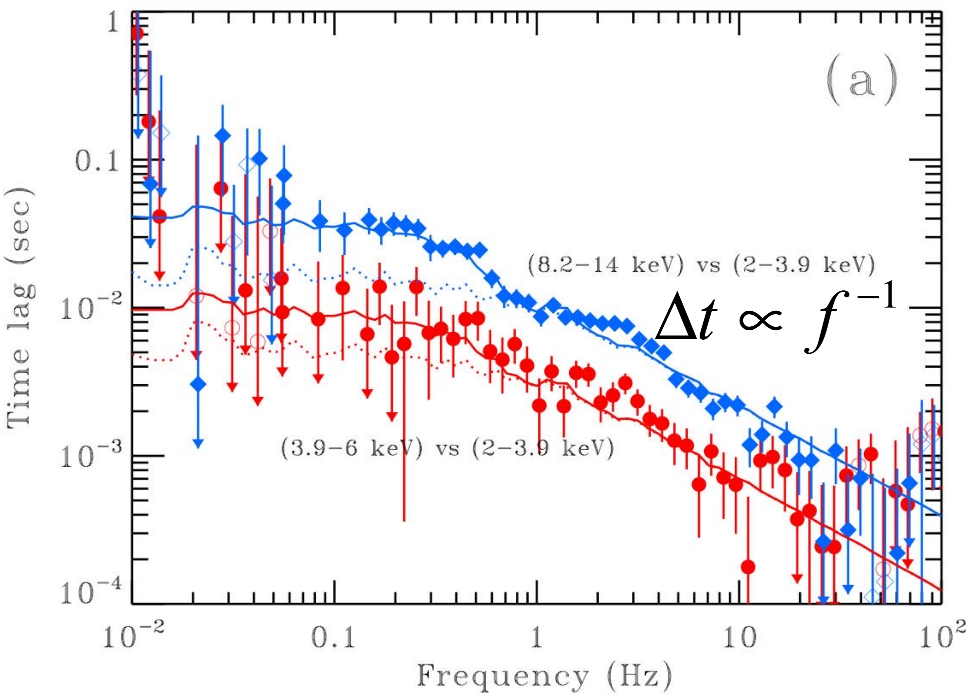

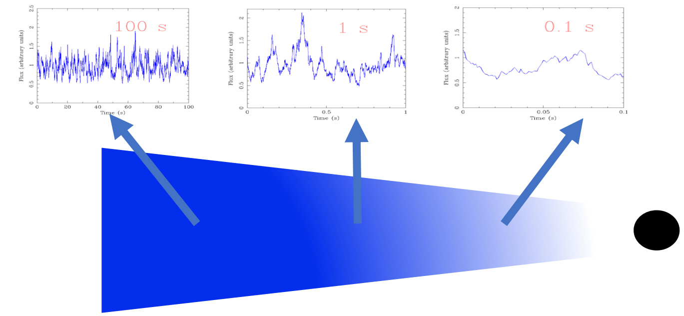

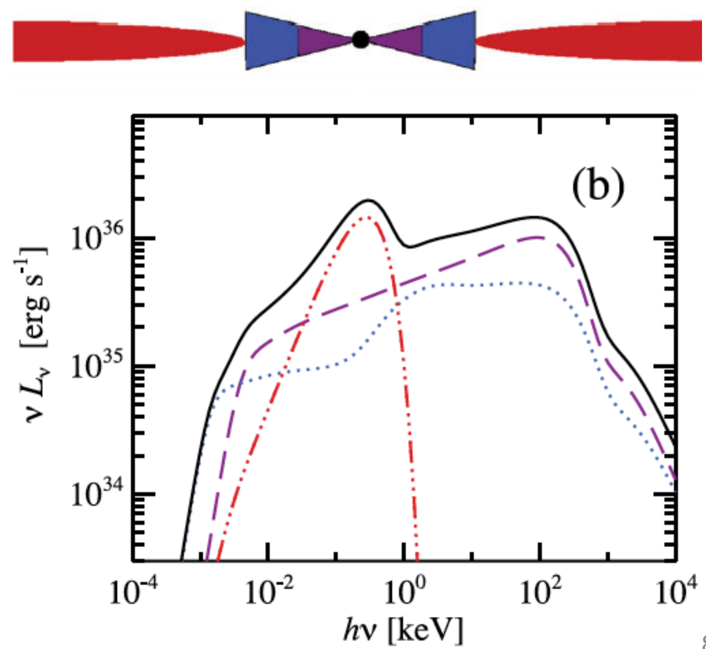

- Cold outer disc+hot inner accretion flow
- Harder spectra for smaller regions
- Time lags are inverse of the characteristic local frequency

Time lags in Cyg X-1. Propagation model

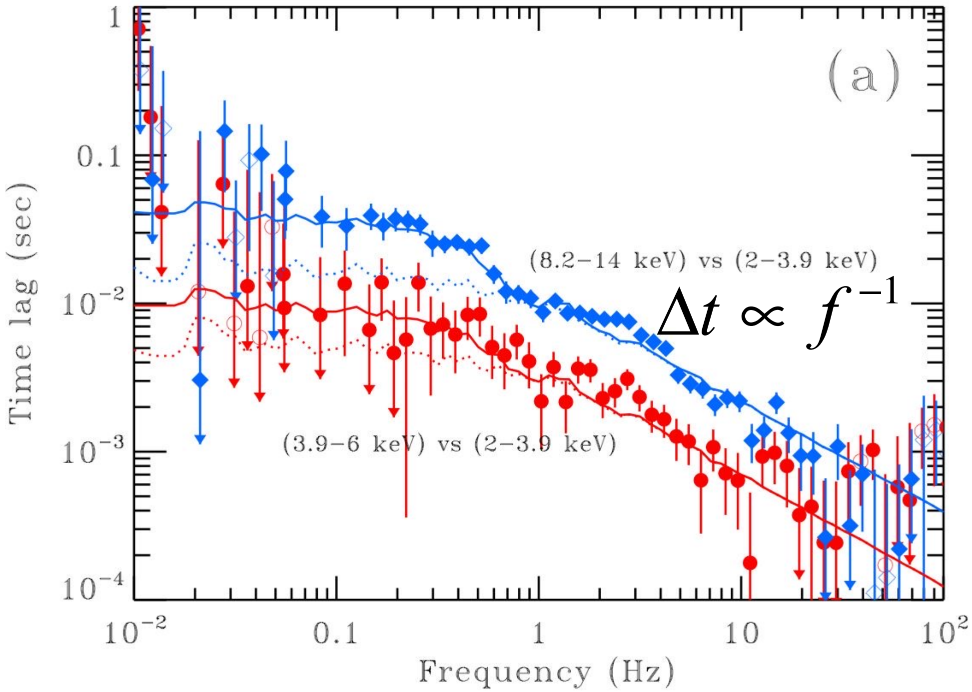

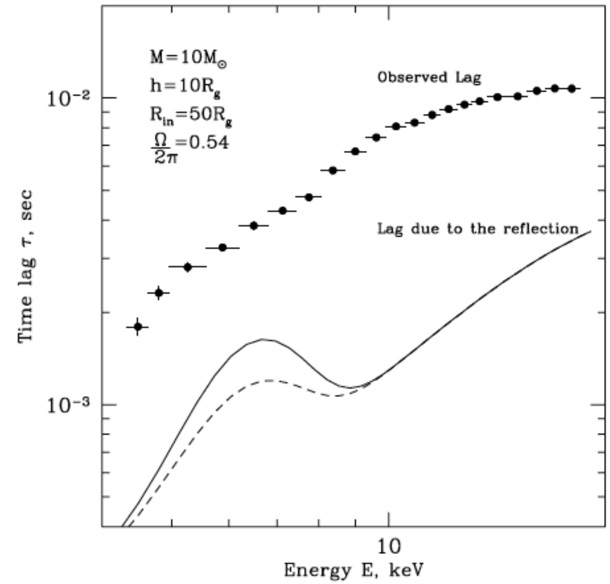

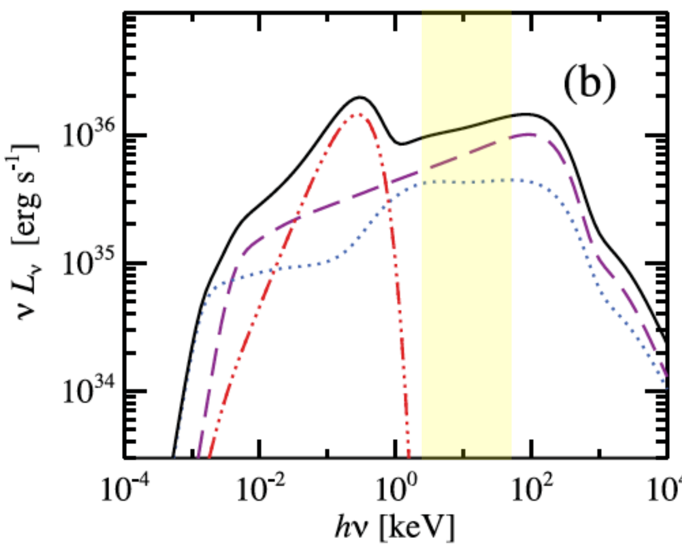

- Cold outer disc+hot inner accretion flow
- Harder spectra for smaller regions
- Time lags are inverse of the characteristic local frequency

Time lags at soft energy bands. Reverberation

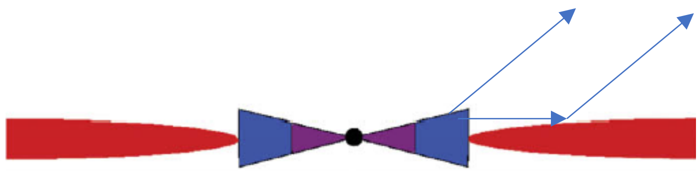

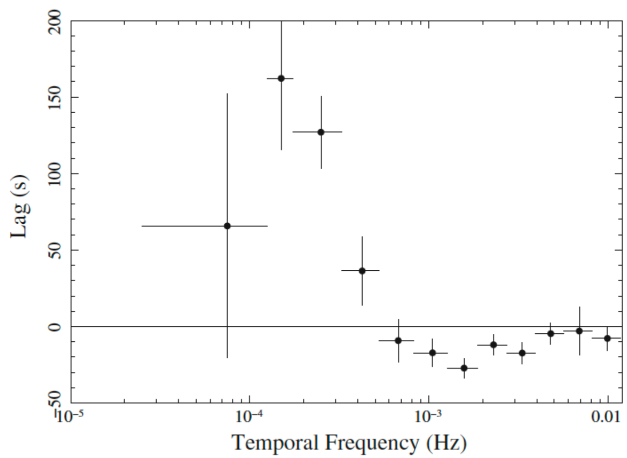

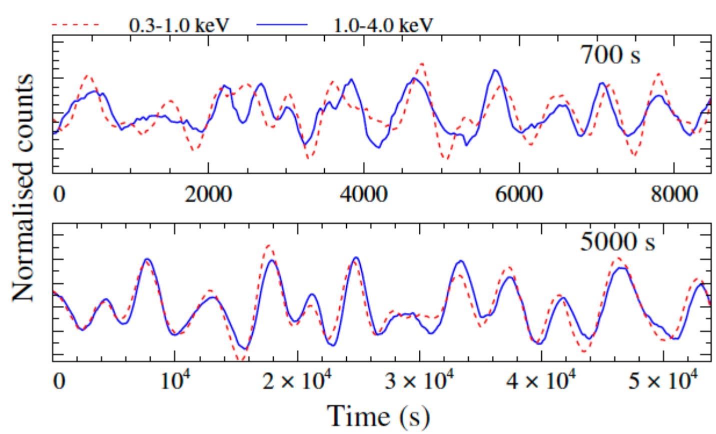

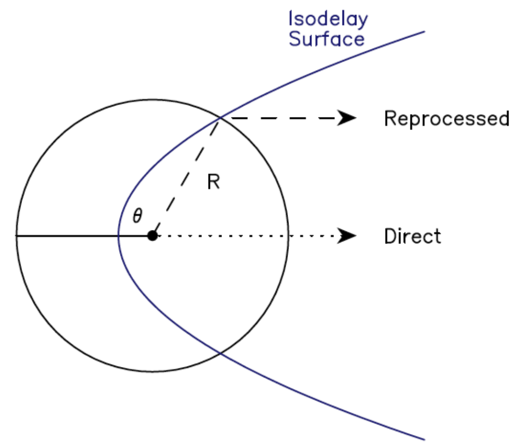

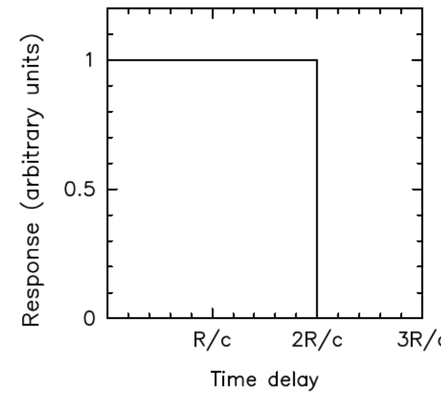

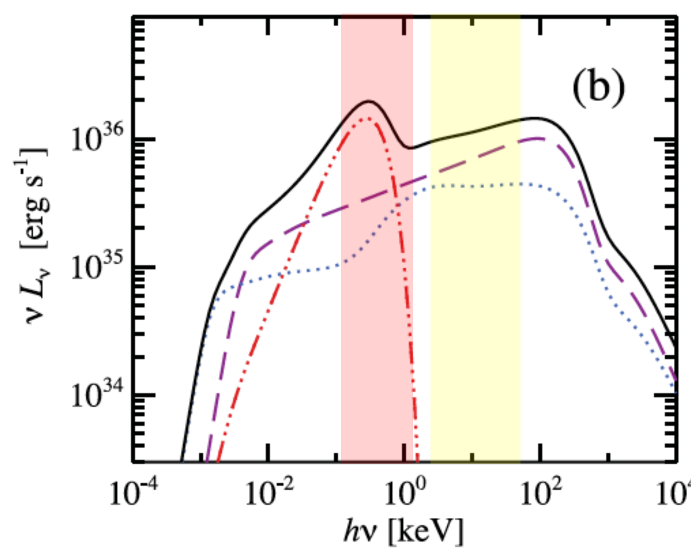

Time lags at soft energy bands. Reverberation

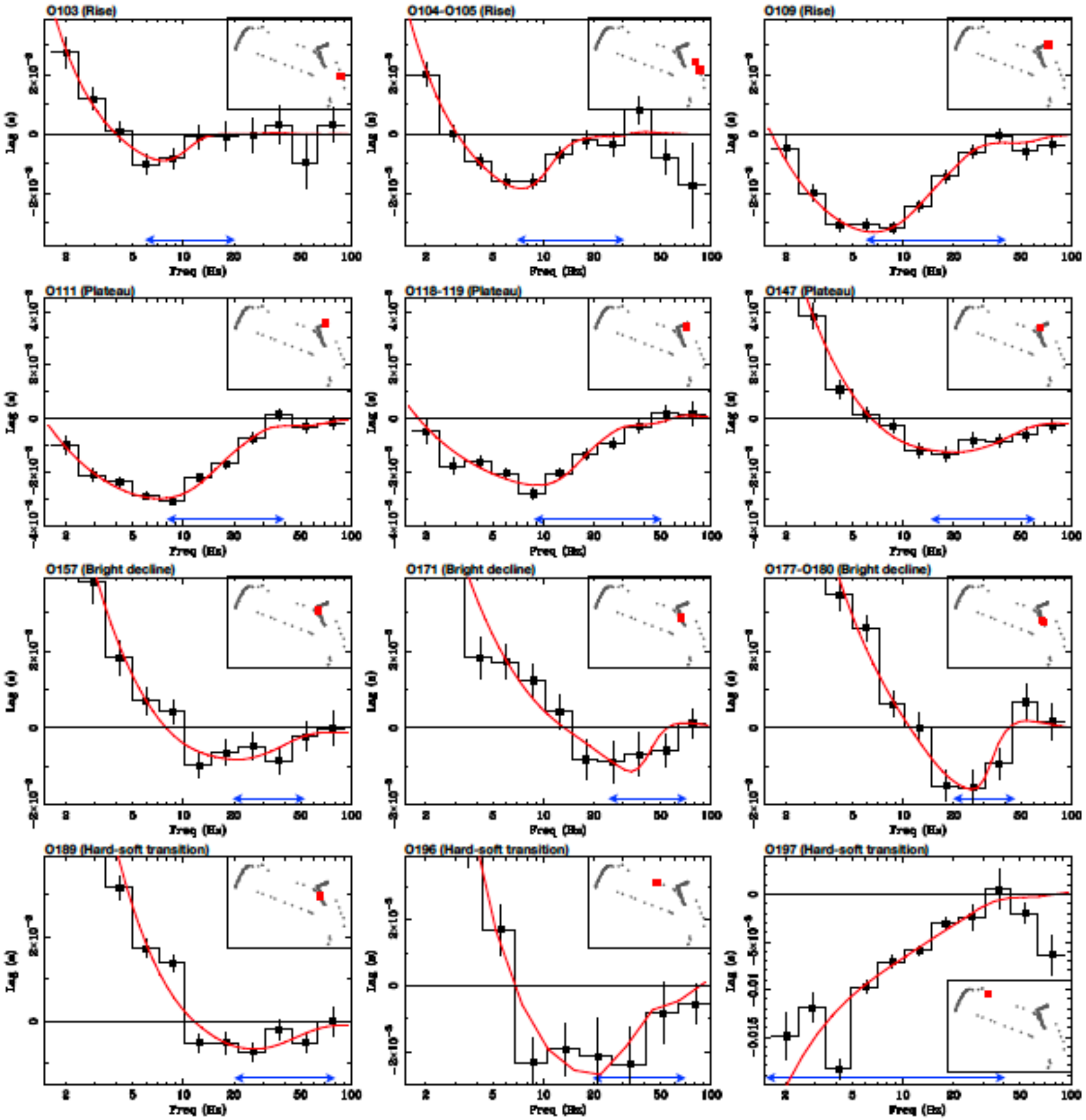

Black hole quasi-periodic oscillations

- QPOs = quasi-periodic oscillations
- Peaks in the power spectra, broader than the window function, but narrower than the peaked noise
- Can be described by Lorentzian profile:

$$P(\nu) = \frac{r^2\Delta}{\pi}\frac{1}{\Delta^2 + (\nu - \nu_0)^2}$$

- Characterized by quality factor:

$$Q \equiv \nu_0/2\Delta$$

- Frequency of maximal power:

$$\nu_{\max} = \sqrt{\nu_0^2 + \Delta^2} = \nu_0\sqrt{1 + \frac{1}{4Q^2}}$$

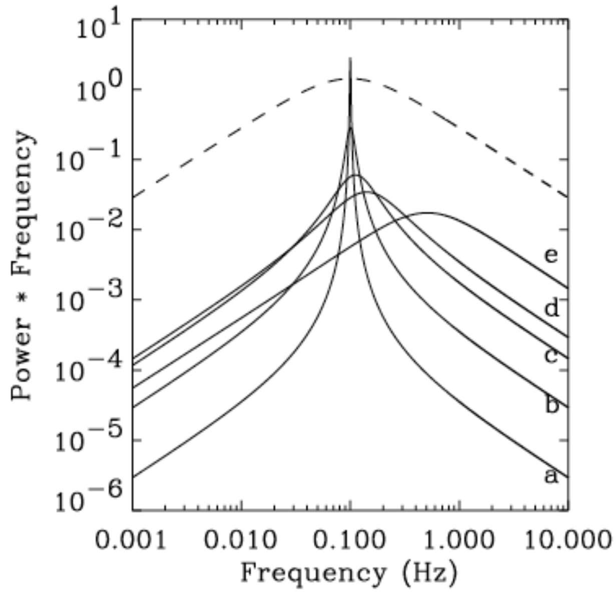

$Q = 50, 2, 1, 0.5, \text{and } 0.1$

Black hole quasi-periodic oscillations

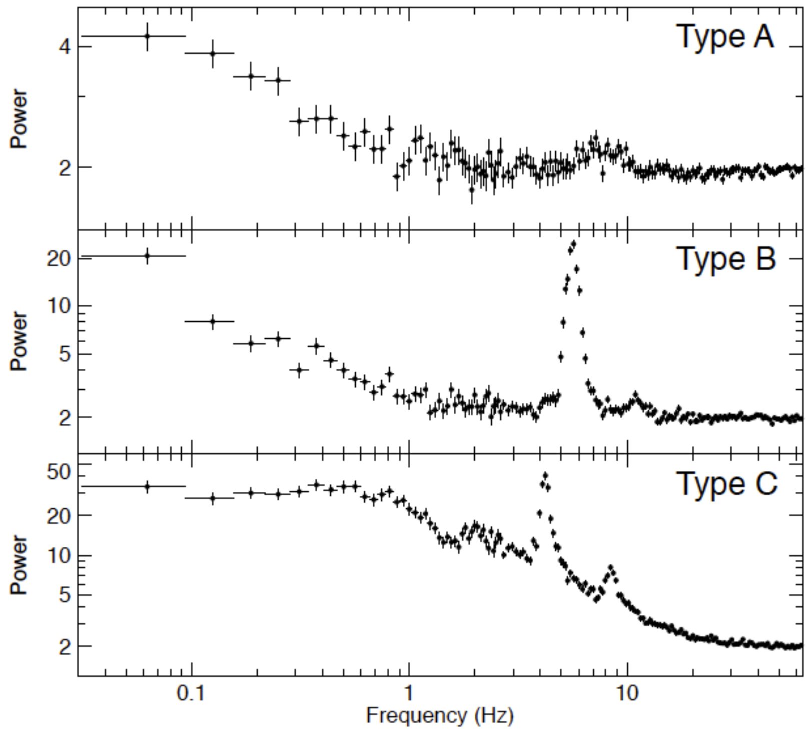

Low-frequency QPOs

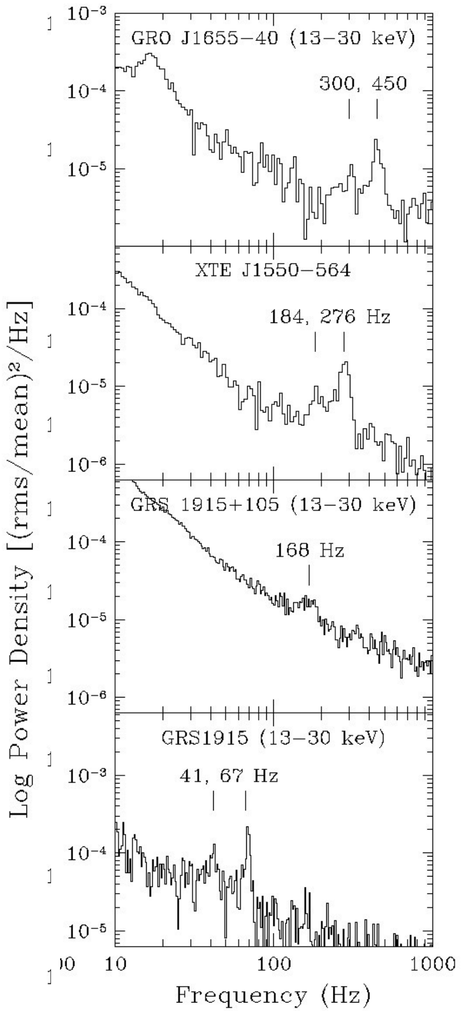

High-frequency QPOs

Relativistic precession model for low-frequency QPOs

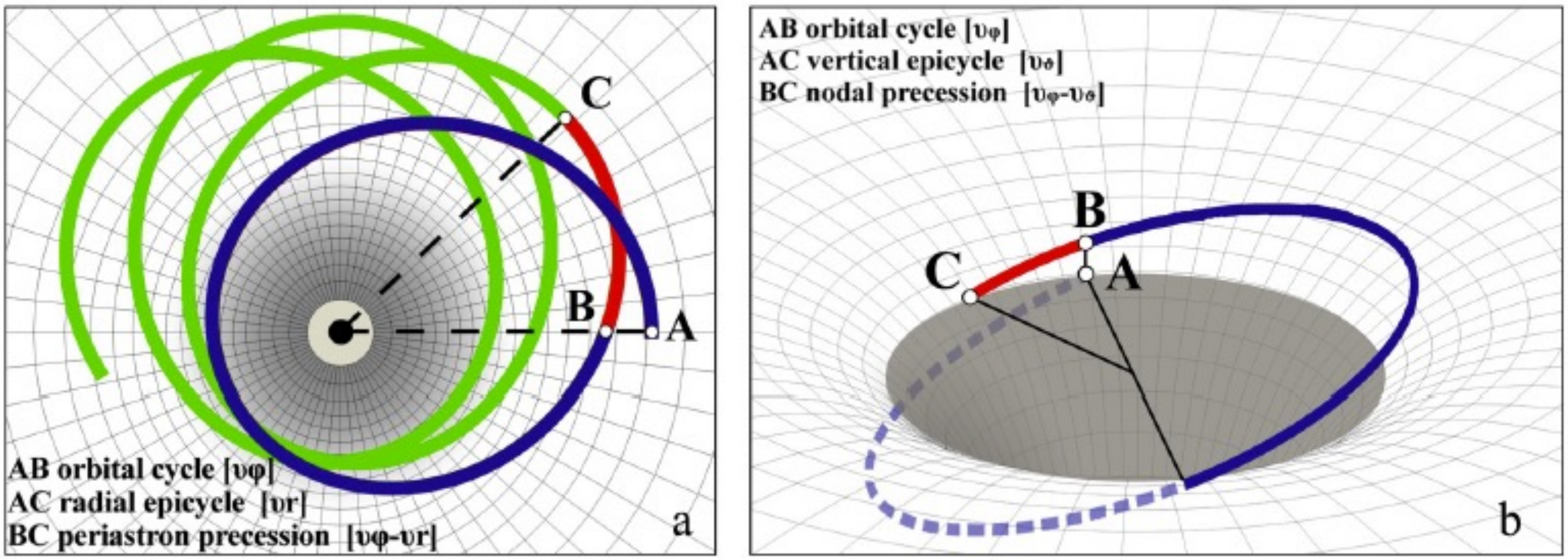

Fig. 1 Example of an eccentric and tilted orbit around a Kerr black, as seen face on (left panel), and from a $\sim$ 60 deg inclination angle (right panel). Cycles are represented for each of the three different fundamental frequencies of motion: azimuthal (aka orbital), and radial epicyclic and vertical epicyclic. The way in which the orbit undergoes periastron and nodal precession is also shown. Embedding diagrams are plotted to help visualize the perspective.

Relativistic precession model for low-frequency QPOs

$$\nu_\phi = \pm \frac{1}{2\pi} \left(\frac{M}{r^3} \right)^{1/2} \frac{1}{1 \pm a \left(\frac{M}{r} \right)^{3/2}}$$

$a = Jc/GM^2$

Units: $c = G = 1$

$$\nu_r = \nu_\phi \left(1 - \frac{6\,M}{r} - 3a^2 \left(\frac{M}{r} \right)^2 \pm 8a \left(\frac{M}{r} \right)^{3/2} \right)^{1/2}$$

$$\nu_\theta = \nu_\phi \left(1 + 3a^2 \left(\frac{M}{r} \right)^2 \mp 4a \left(\frac{M}{r} \right)^{3/2} \right)^{1/2}$$

Relativistic precession model for low-frequency QPOs

$$\boxed{\nu_{\rm per} = \nu_\phi - \nu_r}$$

- Mercury perihelion advance: 43” per Julian century
- Binary pulsar PSR 1913+16 (Hulse-Taylor pulsar): 4.2^o per year
- Double supermassive black hole OJ 287: 39^o per orbit (12 years)

Relativistic precession model for low-frequency QPOs

$$\boxed{\nu_\theta = \nu_\phi \left(1 + 3a^2 \left(\frac{M}{r}\right)^2 \mp 4a \left(\frac{M}{r}\right)^{3/2}\right)^{1/2}}$$

$$\boxed{\nu_{\rm nod} = \nu_\phi - \nu_\theta}$$

Lense-Thirring precession

- The BH and orbital spins are misaligned
- BH is dragging the space-time -> precession
- If t_{LT}>t_{sound}, then a solid body precession

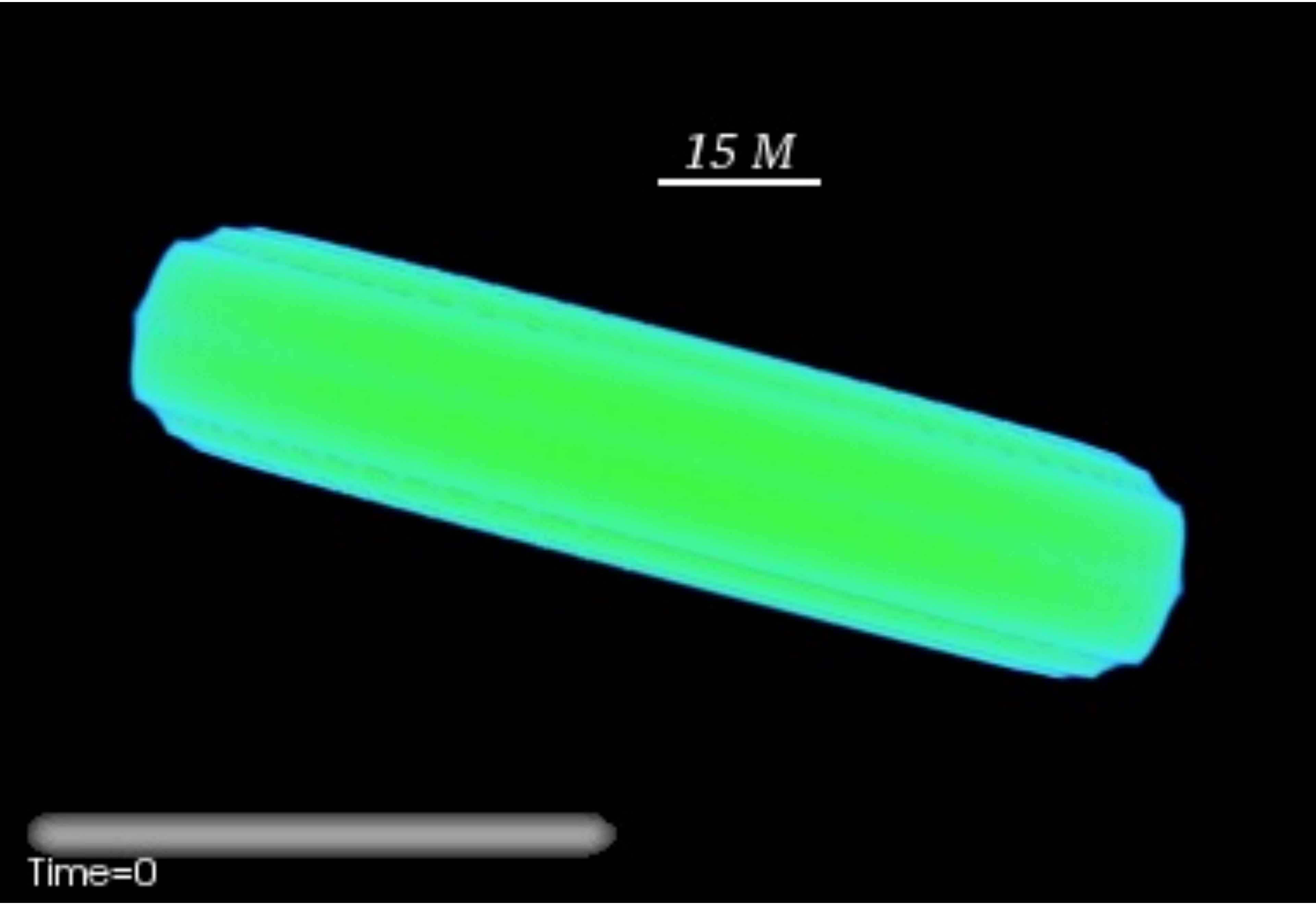
15 M
Time=0

Simultaneous changes of QPO frequency, low-frequency break of the PSD and the spectral softening

- Low-frequency QPO moves in frequency as the spectrum softens/hardens
- QPO frequency is correlated with the low-frequency break of the power spectrum
- Plausible explanation: changes of the disc truncation radius

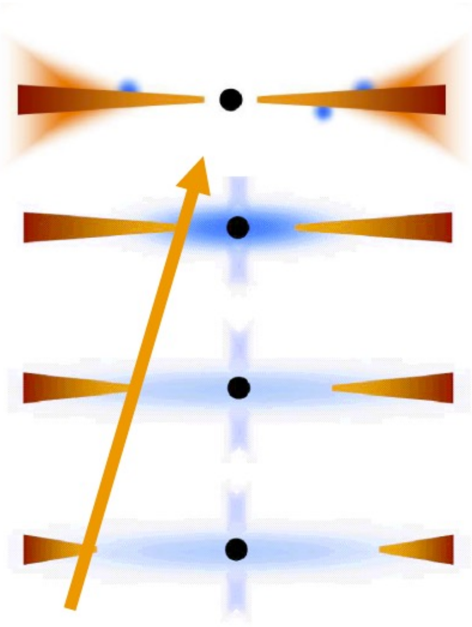

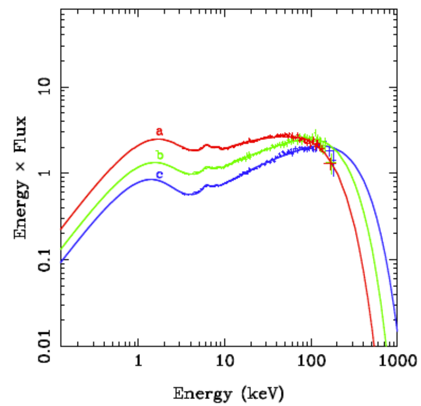

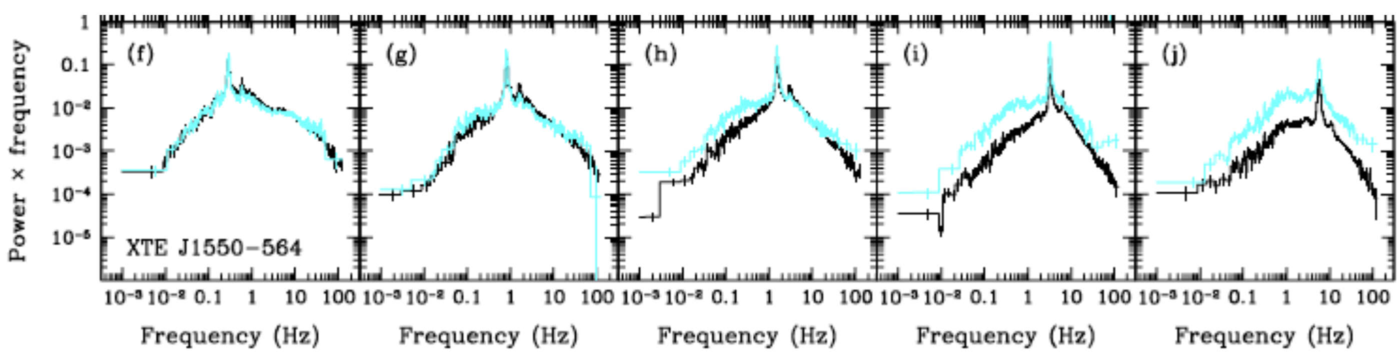

Quasi-periodic oscillations in neutron stars

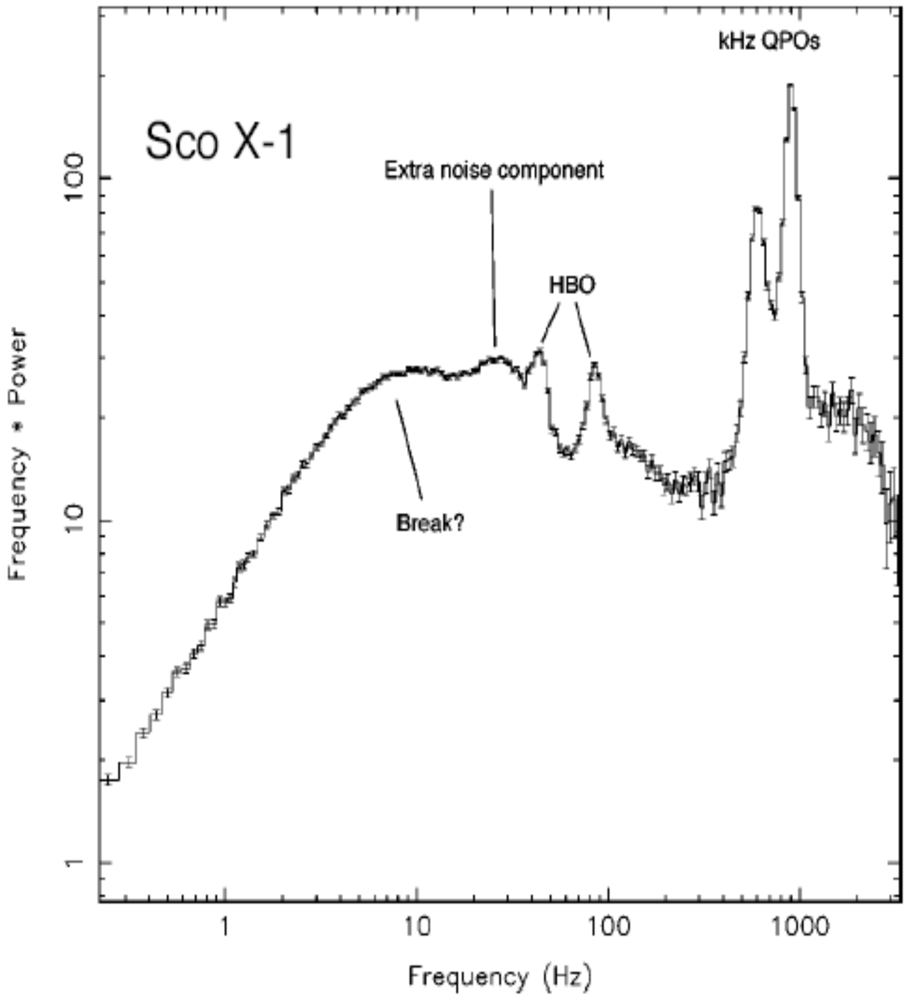

X-ray flux power density spectrum

Kilohertz QPOs have now been detected in some 25 neutron stars

The oscillations are remarkably coherent ($Q = \nu/\delta\nu \sim 30$–$200$)

Two simultaneous kilohertz QPOs are usually seen

The frequencies of the two QPOs sometimes vary by many hundreds of Hz in a few hundred seconds

The separation $\Delta\nu_{QPO} = \nu_{QPO2} - \nu_{QPO1}$ of the two QPOs remains fairly constant, either $\approx \nu_{spin}$ or $\approx \nu_{spin}/2$

Frequency-resolved spectroscopy

- Assume the spectral variability can be represented as

$$S(E,t) = S_0(E) + S(E)f(t)$$

- The Fourier transform is
$$\hat{S}(E,f) = S(E)\hat{f}(\nu)e^{i\varphi(\nu)}$$
- And the power spectrum

$$P(E,\nu) = S^2(E)\left|\hat{f}(\nu)\right|^2$$

Boundary layer and disk in NS

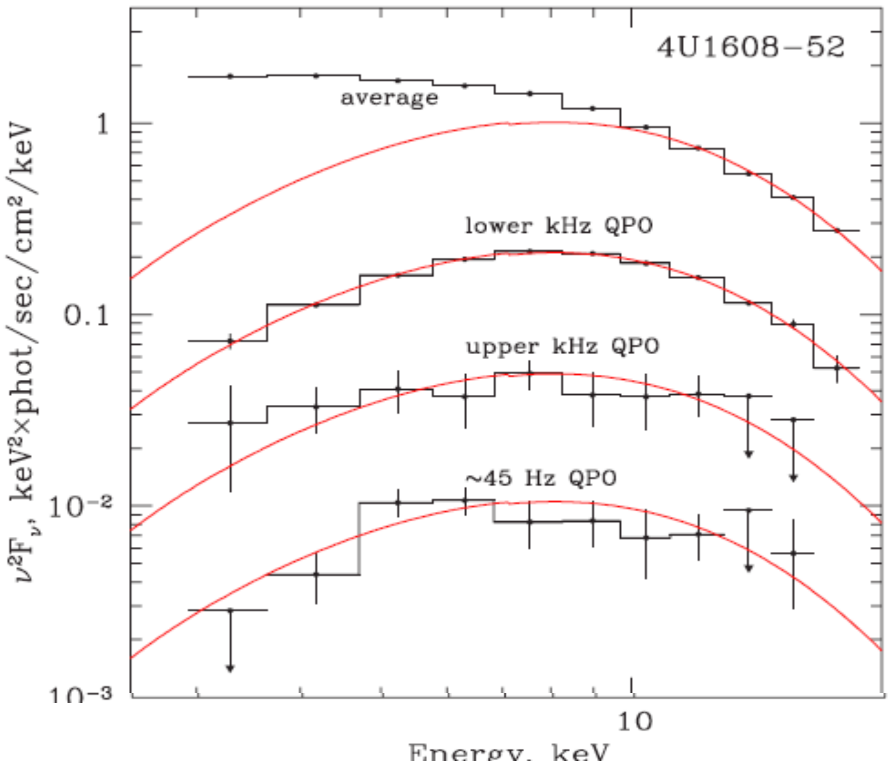

$$R = N_\gamma / T$$

$$P_j = 2|a_j|^2 / N_\gamma R$$

$$a_j = \sum_{k=1}^{2^m} x_k e^{i\omega_j t_k}$$

$S(E_i, f_j)$ is the countrate of the spectrum at frequency f_j in the energy chanel E_i

Fourier frequency resolved spectra

$$S(E_i, f_j) = R_i \sqrt{P_i(f_j)\Delta f_j} = \sqrt{\frac{2|a_{ij}|^2}{T}\Delta f_j}.$$

Boundary layer and disk in NS

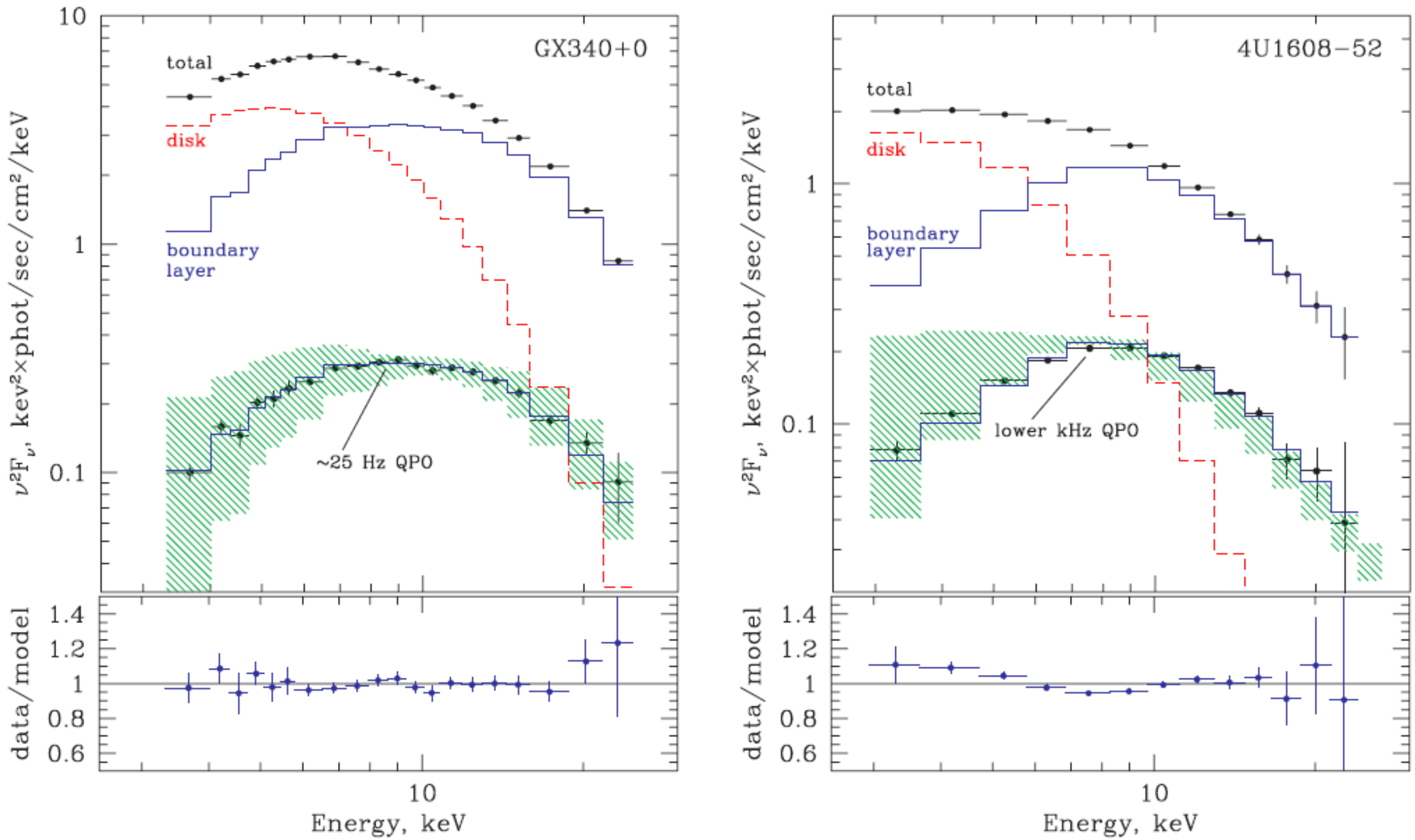

Fourier frequency resolved spectra

$$S(E_i, f_j) = R_i \sqrt{P_i(f_j)\Delta f_j} = \sqrt{\frac{2|a_{ij}|^2}{T}\Delta f_j}.$$

Boundary layer and disk in NS

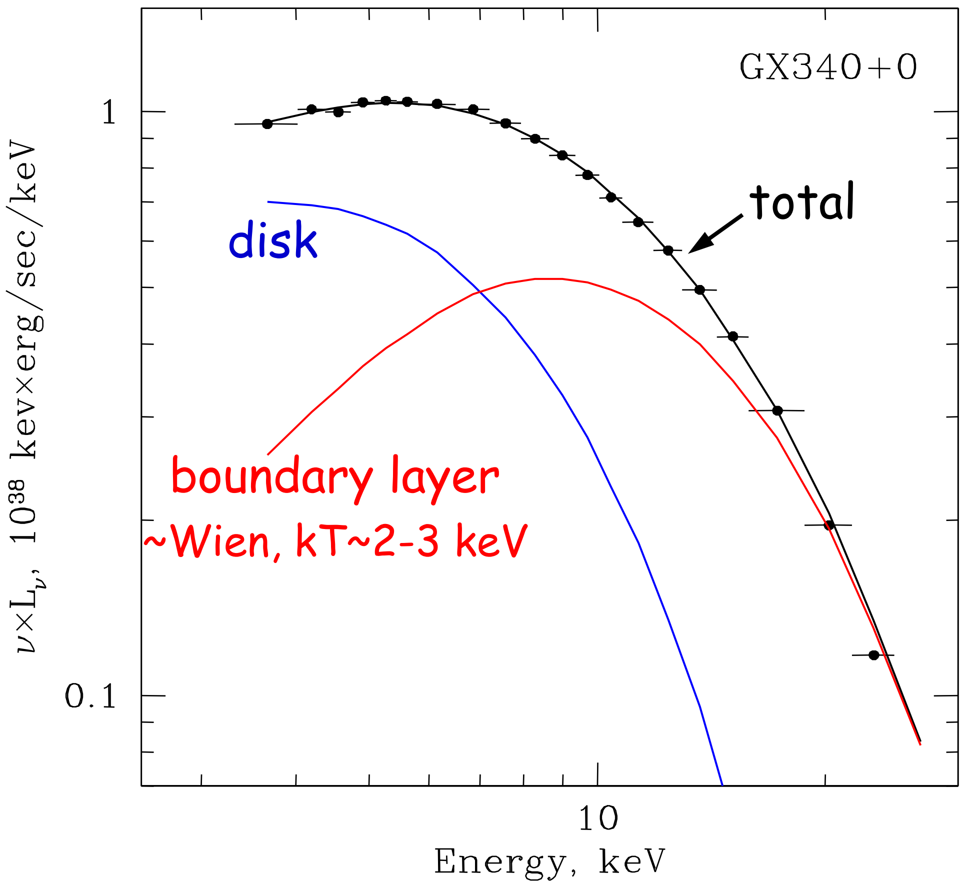

Fourier frequency resolved spectroscopy shows that boundary layer produces QPOs

Fourier frequency resolved spectra

$$S(E_i, f_j) = R_i \sqrt{P_i(f_j)\Delta f_j} = \sqrt{\frac{2|a_{ij}|^2}{T}\Delta f_j}.$$